WILEY-VCH

Graphene based printable conductive wax for low-power thermal actuation in microfluidic paper-based analytical devices

R. Brito-Pereira[a,b,c,d], C. Ribeiro[c,d], P. Costa[c,d,e], V. Correia[a,b], V. F. Cardoso[a,b,] and S. Lanceros-Mendez[c,d,f,g,*]*

[a]Center for MicroElectromechanical Systems (CMEMS-UMinho), University of Minho, Campus de Azurém, 4800-058, Guimarães, Portugal
[b]LABBELS-Associate Laboratory in Biotechnology and Bioengineering and Microelectromechanical Systems, Universidade do Minho, Braga/Guimarães, Portugal
[c]Physics Centre of Minho and Porto Universities (CF-UM-UP), Universidade do Minho, 4710-057, Portugal
[d]LaPMET-Laboratory of Physics for Materials and Emergent Technologies, Universidade do Minho, 4710-057, Portugal
[e]Institute for Polymers and Composites IPC/i3N, University of Minho, Campus de Gualtar, Braga, 4710-057, Portugal
[f]BCMaterials, Basque Center for Materials, Applications and Nanostructures, UPV/EHU Science Park, 48940 Leioa, Spain
[g]IKERBASQUE, Basque Foundation for Science, 48009 Bilbao, Spain

E-mails: vcardoso@cmems.uminho.pt (VFC); senentxu.lanceros@bcmaterials.net (SLM)

Keywords: microfluidic, heater, graphene, wax, printing

Wax printing is one of the most widely used techniques to print hydrophobic barriers on hydrophilic microfluidic paper-based analytical devices (µPADs) based on its simplicity, speed and low cost, allowing large-scale production. Nonetheless, its function is just passive, without any action on fluids. Thus, this work proposes multifunctional hydrophobic composites based on conductive graphene nanoplatelets (GNP) integrated into the wax matrix to allow a dual role of barrier and heater, the latter being required in a large variety of temperature-sensitive reactions and microfluidic applications. The effect of GNP weight content on the physicochemical properties of the wax, printed wax and generated heating are evaluated. Wax prints with mechanical stability and adequate impregnation through the paper are obtained after post-thermal curing. With respect to the functional response, controlled temperatures ranging from room temperature to ~107 ºC can be achieved after just 10 s. Two proofs of concept are presented involving thermochromic inks, specific printed systems designs, and low-power batteries. The benefits of µPADs allied to the increased functionality and performance of the developed waxes, hold great promise to meet the requirements for a next generation of versatile, effective and accurate µPADs for an increasing number of applications.

1. Introduction

Paper has been a base material for many applications for centuries. It is based on cellulose, which is a renewable polymer, produced by trees, plants and some non-pathogenic bacteria[1]. Besides being affordable and widely available, this polymer features interesting physicochemical properties such as biocompatibility, flexibility, low weight and hydrophilicity by nature, which results in an effortless fluid flow by capillary action with no need for external pumps or pressure[2,3]. Moreover, it allows modification with a variety of functional groups to perform specific analytical assays[4]. These assets make it suitable for the development of devices, including microfluidic paper-based analytical devices (µPADs), a concept that was introduced in 2007 by Whitesides and co-workers when photolithography was employed to patterned paper and colorimetric analyses were implemented[5]. Although *Whatman nº1* paper is the gold standard used microfluidic substrate, other versions such as *Whatman nº4*, nitrocellulose, bacteria cellulose nanopaper and nylon membranes are also used to develop µPADs[6]. Recently, new polymer-based materials with promising and tailorable physicochemical properties, including controllable flow rates, have been introduced and successfully tested as alternative to the commonly used microfluidic paper substrates[7–10].

µPADs have been initially developed for resources limited environments, in-field applications or for their use in private homes, as they fulfil the ASSURED (i.e. Affordable, Sensitive, Specific, User-friendly, Rapid and Robust and Deliverable) criteria defined by the World Health Organization (WHO) and being therefore suitable for point-of-care (POC) devices development[4]. Thus, their potential has expanded to such an extent that nowadays this technology is used in numerous applications worldwide such as clinical[1], veterinary[11], food industry[12], agriculture[13], biodefense[14], energy[15] and environmental purposes[16], among others[17–19]. Its popularity is due to the fact that µPADs present several advantages comparatively to traditional microfluidic devices made of silicon, glass or other polymers (e.g. polydimethylsiloxane-PDMS), as well as to the conventional laboratory techniques, including low cost, low sample volume consumption, ease of use, portability, *in situ* measurement, high sensitivity, and no need for sophisticated laboratory equipment and trained user[20,21]. Moreover, they can be used not just in lateral flow assays but also for multiplex analysis and complex analysis requiring multiple steps (e.g. sample transport, pre-treatment, mixing, reaction, separation)[22,23]. Thus, significant growth of academic research on paper-based analytical

fabrication methods and integrated tools (e.g, optical sensors, pressure sensors, micropumps, microvalves, heaters, temperature sensors, among others[24]) has been observed for the past decade to increase their functionality and performance. To turn these materials into functional devices, conductive reinforcing fillers are usually added. Of the different materials, carbonaceous are those with greater chemical stability combined with excellent properties and processability. Graphene is a two-dimensional (2D) material that has attracted major interest for applications because of its excellent electrical conductivity and thermal (5000 $W.mK^{-1}$) properties as well as simple processability and compatibility with various polymer matrices, which makes it an outstanding material for printed flexible devices [25,26]. This will allow the development of effective, accurate and standardize µPADs and promote their commercialization, maintaining simplicity and without compromising its cost[27–29].

For instance, given the hydrophilic nature of paper, hydrophobic boundaries with specific patterns are often required to restrict the fluid flow of samples and reagents to specific pathways of the hydrophilic substrate[30]. To address these goals, different strategies have been used such as photolithography, wax printing, inkjet printing and screen-printing. Folding several layers of patterned paper, origami inspired, has also been employed to obtain three-dimensional (3D) µPADs. Several review articles address these techniques in detail[2,22,31–33]. Each of those approaches has its own benefits and limitations, so the choice is often based on cost, substrate, fabrication time, equipment availability and also specific application demands. Photolithography uses a chemical photoresist to infiltrate the paper substrate and create the barrier by exposing the substrate to light through a photomask. This technique presents good resolution but suffer from the cost of the photoresist and organic solvent, fragile nature of the resulting devices and possible production of background signals[4]. A technique that has become popular to pattern channels in µPADs is wax printing. Although the printing resolution cannot be compared with photolithography, the production steps are simpler, faster and cheaper, being, thus, best suited for large scale production[34]. It involves a three-step method including the pattern drawing using an appropriate software, the paper printing using a commercial wax printer and the heating step to allow impregnation of the wax through the paper to the opposite surface[35]. Moreover, wax-based devices are mechanically resistant and are compatible with lamination allowing to fabricate complex 2D or 3D structures for multipurpose applications[30].

Nonetheless, despite the excellent quality of wax printing that makes it one of the materials and techniques most used in the manufacture of µPADs systems, its function is passive, working only as boundaries to delineate hydrophilic channels without any action on the fluids. On the other hand, thermal actuators are commonly needed in microfluidic technology for precise temperature-sensitive reactions and applications such as colorimetric analytic analysis[9,36], cell culture[37,38], polymerase chain reaction[39,40], cell lysis[41,42], among others technological applications. However, they are still not well developed for µPADs. As instance, heaters were implemented in µPADs in the forms of non-contact inductive heater[43], laser heater[44,45], infrared heater[46], and microwave heater[47,48], among others, being resistive heaters[24,49,50] the most commonly used due to their low fabrication cost and mature fabrication process. Due to its intrinsic properties, graphene has been used as reinforcing material in a variety of polymer matrices, leading to improved mechanical and electrical properties [26], as well as high thermal conductivity in composite materials [51,52]. However, they required additional processing techniques for their proper integration into µPADs.

In this context, the present work reports on the implementation of active functionalities to the hydrophobic wax through the integration of conductive graphene fillers, on behalf of their electrical and thermal conductivity and good mechanical properties[53–55]. Conductive wax and printed patterns have been developed, the latter with the individual or dual function of barrier and heater using a simple, single and rapid fabrication method.

2. Experimental

2.1. Materials

Whatman nº1 cellulose paper was purchased from *Sigma-Aldrich* (Missouri, USA). Graphene nanoplatelets (GNP) characterized by 2-30 layers with <10 nm of thickness and 1-20 µm of particle size were supplied by *Graphenest* Company (Sever do Vouga, Portugal). Commercial black dye wax cartridges were obtained from *Xerox Corporation* (Connecticut, USA). This solid wax is composed by about 60% of paraffin wax, 20% of polyethylene resin, and about 10% of black dye. Thermochromic Inks were purchased from *SFXC-Good Life Innovations Ltd* (Denton Island, UK), namely: two temperatures responsive thermochromic inks – red to more translucent (light rose) when activated at temperatures higher than 28 and 47 ºC, respectively, and temperature responsive thermochromic ink – green to yellow when activated at temperature higher than 28 ºC.

Pure ethanol (99 %) was obtained from *Sigma-Aldrich* (Missouri, USA). 1.5, 9 and 12 V alkaline batteries were supplied from a local store. All materials were used as received from the providers.

2.2. Experimental methods

2.2.1. Conductive wax preparation

For the preparation of the GNP/Wax composites, GNP was added to 15 mL of pure ethanol at a defined concentration (Figure 1a). The solutions were placed in an ultrasonic bath (*Fisherbrand, FB15056*) for 3 h to avoid agglomeration between GNP and ensure their proper dispersion (Figure 1b). Previously cut Xerox wax of ~45 g was then added to the mixture (to obtain a final GNP weight percentage of 5, 10, 15 and 20 wt.%) and placed in an oven (*JP Selecta, 2000208*) for 30 min at a temperature of 120 ºC, to ensure suitable polymer melting and complete evaporation of the solvent (Figures 1c and 1d). Then, the GNP/Wax mixture was removed from the oven and placed in a hot plate (*Prazitherm P272*) at the same temperature and mixed with the help of a mechanical Teflon stirrer (*Heidolph RZR 1*) for 1 h at 100 rpm to ensure the homogeneity of the melt composites (Figure 1e). Finally, each melted mixture was poured into a homemade aluminium mould, specially designed and manufactured to ensure a shape compatibility with a commercial wax printer (*Xerox Colorqube 8880*). The mould was allowed to cool down to room temperature (~25 ºC) for 10 min and dissembled, being the obtained solidified GNP/Wax cartridges ready to be introduced into the printer (Figure 1f).

2.2.2. Printing process

Various neat wax and GNP/Wax designs with defined dimensions were created, according to the intended application (described in Sections 2.3 and 2.4), using a computer-assisted design software (*Sketchup 2017*) and printed with a *Xerox ColorQube 8880* printer (during printing the cartridge melts at temperature higher than 100 ºC) on the *Whatman nº1* cellulose paper substrates (uncured samples) (Figure 1g). After printing, the samples were placed on a hot plate for a thermal cure at 100 ºC for 5 min, allowing the wax to penetrate the substrates all the way through to the opposing surface (cured samples)[56,57] (Figure 1h).

The following nomenclature will be used to facilitate the identification of the waxes in the Figures: Uncured and cured samples will be identified as "Unc." and "C.", respectively, the concentration of GNP as "weight percentage"GNP/Wax and when the wax is printed the identification "@Paper" is added.

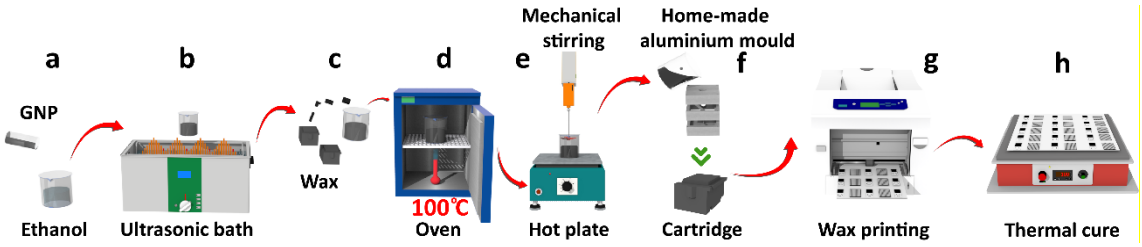

Figure 1: Schematic representation of the preparation of the GNP/Wax cartridges and the corresponding printing process.

2.3. Samples characterization

2.3.1. Rheological characterization

Rheological properties of different prepared waxes were evaluated using an *Ares-G2* rheometer equipped with a flat plate geometry (40 mm) and a gap of 500 μm. A steady shear flow test was carried out at 100 ºC, with a shear rate range from 0 to 500 s^{-1}. Accordingly, the melted waxes' viscosity as a function of the shear rate was obtained.

2.3.2. Contact angle characterization

Moreover, drops with approximately ~10 μL from different melted waxes (~100 ºC) were deposited on the surface of *Whatman nº1* paper at a temperature of 30 and 80 ºC, and the contact angles were evaluated using a *Data Physics OCA20* instrument. Four measurements were performed in each case at different locations, and the contact angles being reported as the average and standard deviation.

2.3.3. Morphological characterization

The surface and cross-section morphologies of printed and cured waxes were assessed with a *NanoSEM - FEI Nova 200* (FEG/SEM) scanning electron microscope at 10 kV.

Before SEM, samples were gold coated by magnetron sputtering using a *Polaron SC502* sputter coater.

2.3.4. Adhesion assays

The adhesion of the different printed waxes on *Whatman nº1* paper was studied with an adapted tape peel test [58] performed on samples with an area of 10×10 mm^2. For that, an adhesive tape (*3 M Scotch® Magic™ tape 810*) was pressed on the surface of the printed samples with different forces (50, 100, 150 and 200 N for 30 s) using a *Shimadzu AG-IS* universal test set-up, in compression mode at 2 $mm.min^{-1}$. After that, the tape was removed from the sample at the same speed, while monitoring the force applied to the sample. Each sample was weighed before and after each assay (subtracting the paper substrate weight), to determine the percentage of wax mass loss.

2.3.5. Stress-strain mechanical measurements

The mechanical properties of the different printed waxes on *Whatman nº1* paper (30 mm long and 10 mm wide) were obtained by uniaxial stress–strain measurements in tensile mode at a deformation rate of 0.5 $mm.min^{-1}$ and at room temperature (~25 ºC) using a *Shimadzu* model *AG-IS* and a load cell of 500 N. Three assays were carried out for each sample. The elastic modulus, Y, was calculated in the linear regime until 0.5 % of the stress (σ)–strain (ε) curves after Hooke's law (equation 1):

$$\sigma = Y \cdot \varepsilon \quad (1)$$

2.3.6. Electrical conductivity assays

Sheet resistance measurements were performed using silver paint electrodes (AGG3790, *Agar Scientific*) with area of 2×1 mm^2 and distance of 10 mm between them. The DC electrical voltage was varied from -10 to +10 V in steps of 1 V measuring the current using a *Keithley 487* picoammeter/voltage source. The surface electrical resistivity (σ) and conductivity (ρ) were determined from the linear slope of the I-V curves after equation 2:

$$\sigma = \frac{1}{\rho} = \frac{1}{R}\frac{d}{l} \quad (2)$$

where R is the electrical resistance, d the distance and l the length of electrodes.

2.3.7. Thermal evaluation

Thermal measurements were performed on printed wax lines (15 mm long and 1 mm width) on *Whatman nº1* paper. A temperature probe type *K* (-40 to 260 ºC, ± 0.75 %) *UNI-T UTT10K* connected to *Rigol DM3068 Digital Multimeter* was used. A DC power supply, *21N155 Hikari HF-3203S*, ranging from 0 to 15 V, was used to supply and control the energy provided to the printed lines. Moreover, the temperature was measured as a function of time (30 s). Finally, the temperature was also measured at a distance of 1 and 2 mm from the printed lines (after 10 s, separately) in order to study the propagation of the heating through the paper.

2.4. Functional proofs of concept

Two functional proofs of concept were demonstrated (Figure 2). The first one consists on *Whatman nº1* paper devices with arrays of 6 parallel channels (2 mm width) delimited by neat wax and conductive 20 wt.% GNP/Wax lines (1 mm width) allowing for individualized actuation with different electrical voltages (Figure 2a). In this case, a unique DC power supply was used and applied to different conductive lines. Two different thermochromic inks (green and red) with different activation temperatures at 28 and 47 ºC were used for this purpose.

The second proof of concept consists in the development of a portable printed folded *Whatman nº1* paper device, in which a small battery (1.5, 9 or 12 V) is connected to the heating zone made of conductive 20 wt.% GNP/Wax (with 10×10 mm^2) to generate and provide heat to fluids (in this specific case thermochromic inks) contained in the circular testing area (8 mm diameter) delimited by neat wax (Figure 2b). To build the structure that incorporates the different alkaline batteries and supports the paper device, 3D printing was used (*Prusa* i3 MK3) to obtain an adequate polylactic acid (PLA) support. Two different thermochromic inks (both red) with different activation temperatures at 28 and 47 ºC were used to visually evaluate and validate the developed system. Further, a thermal imaging camera (HT 19 from *HTi*) was also employed in both proof of concepts.

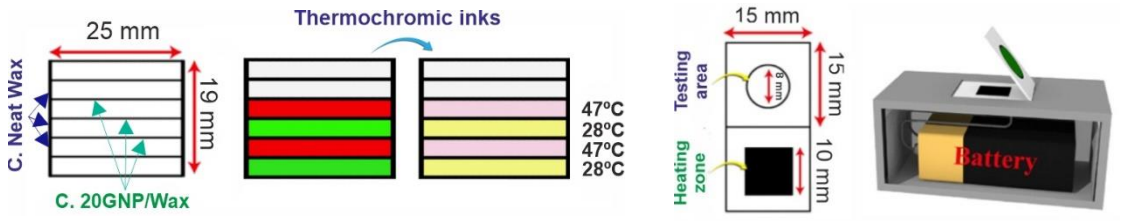

a) b)

Figure 2: Representative illustration of the: a) *Whatman nº1* paper devices with arrays of 6 parallel channels and b) portable printed folded *Whatman nº1* paper device, in which a small battery is connected to a conductive square located underneath the testing area.

3. Results and discussion

3.1. Physicochemical characterization

In order to evaluate the waxes printability, their viscosities were evaluated at 100 ºC as a function of shear rate through a steady shear test (Figure 3a).

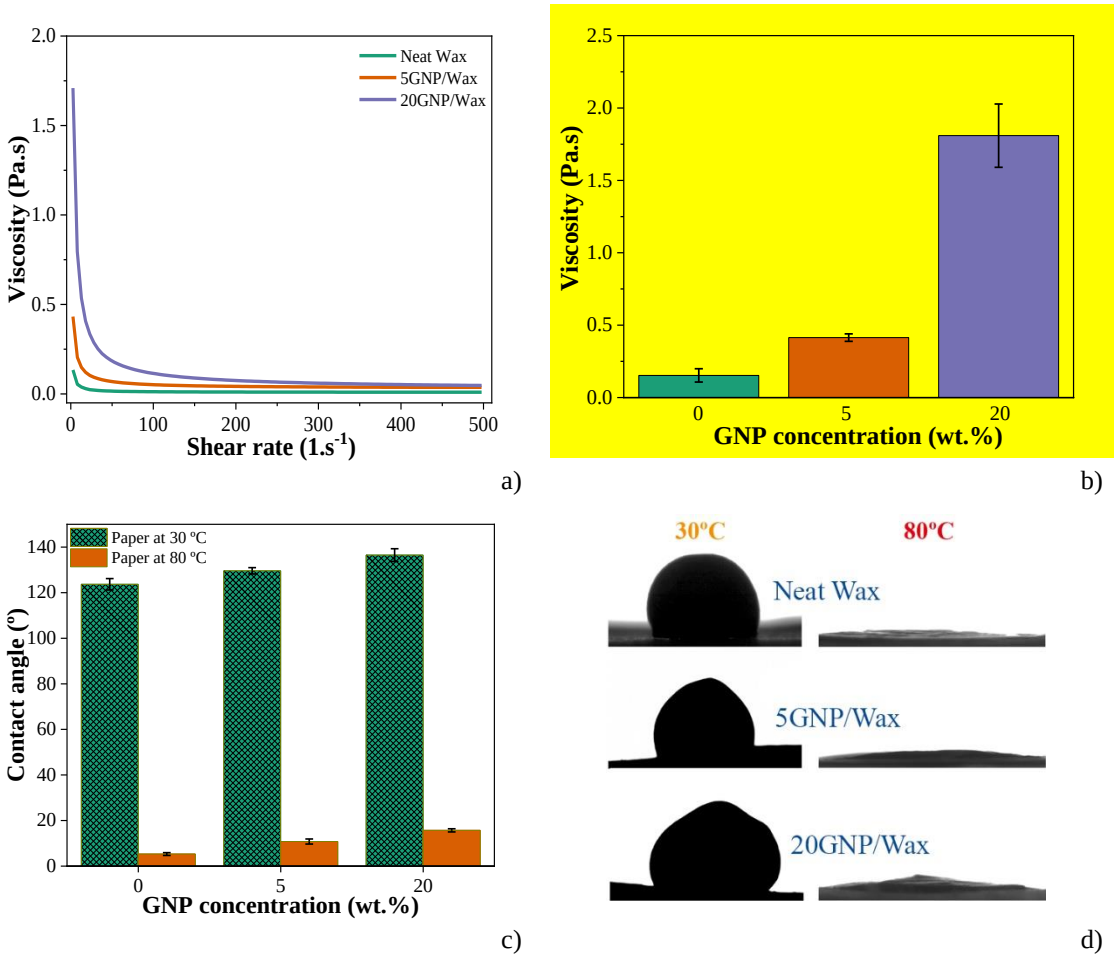

a) b)

c) d)

Figure 3: a) Variation of viscosity of the melted waxes as a function of shear rate for solutions with different GNP/Wax concentrations. b) Viscosity at 2 s^{-1} shear rate for solutions with different GNP/Wax concentrations. c) Contact angle between different melted GNP/Wax concentration drops and paper at 30 ºC (left) and 80 ºC (right); d) corresponding representative photographs of the waxes in contact with paper.

The results demonstrate a typical shear thinning behaviour for the different melted waxes, independently of the filler concentration, as the viscosity decreases by increasing the shear rate. It is also verified that for higher shear rates, all the waxes present similar viscosities, ensuring a printing quality of the developed GNP/Wax similar to the melted neat wax. On the other hand, viscosities are quite different at lower shear rates, based on the different filler content and the interaction of the GNP loading with the polymer matrix. In this way, the viscosity of the different melted waxes at the shear rate of 2 s^{-1} is compared and presented in the Figure 3b. The melted neat wax presents the lowest viscosity (0.15 ± 0.05 Pa.s) and the melted wax with higher concentration of GNP (20 wt.%) the higher viscosity value (1.81 ± 0.22 Pa.s).

In order to evaluate the spreading of the produced waxes on the *Whatman nº1* cellulose paper, contact angle experiments were conducted with the paper at temperatures of 30 and 80 ºC (Figures 3 c and 3d). It is shown that increasing paper substrate temperature leads to an increase of the impregnation of all the waxes, as indicated by the variation of the contact angle from 123.7º±2.5º to 5.3º±0.6º in the case of neat wax, from 129.6º±1.4º to 10.8º±1.1º in the case of 5 wt.% GNP/Wax and from 136.5º±2.8º to 15.7º±0.7º in the case of the 20 wt.% GNP/Wax. New measurements performed around 4 months later demonstrate the stability of the materials and prints over time, with no relevant contact angle values variations over time (all values being within experimental error).

Therefore, to ensure a high impregnation of the printed waxes on the paper substrate, they will be thermally cured at a temperature higher than 80 ºC after the printing procedure.

Representative surface and cross-section SEM images of *Whatman nº1* paper substrate, printed and cured neat wax and conductive 5 and 20 wt.% GNP/Wax on paper are presented in Figure 4. All waxes were properly cured to cross the paper substrate all the way through the opposite surface, so barriers can fully contain fluids if needed.

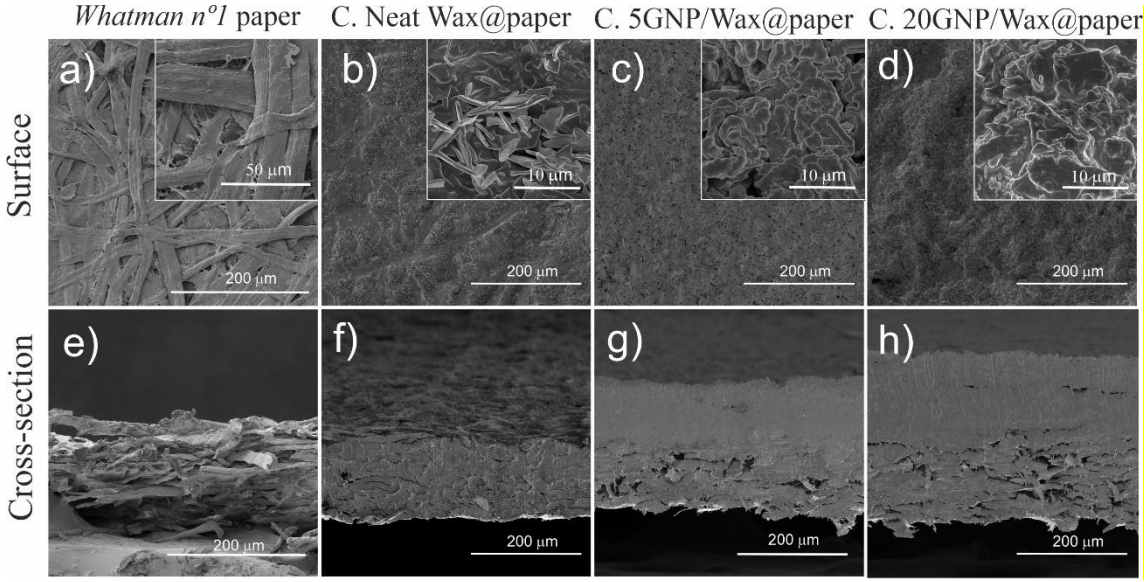

Figure 4: Representative surface SEM images of: a) *Whatman nº1* paper; b) printed cured neat wax on paper; c) printed cured 5 wt.% GNP/Wax on paper; d) printed cured 20 wt.% GNP/Wax on paper. e)-h) Corresponding representative cross-section images.

Whatman nº1 substrates are characterized by non-oriented and flattened cellulose fibres (Figure 4a), which are associated with the fabrication process employed in the manufacture of paper, as reported in [7]. This fibrillar microstructure is evidenced in the transverse image illustrated in Figure 4e. On the other hand, a rough surface (Figure 4b) and compact transversal section (Figure 4f) is obtained after the printing and cure of neat wax on paper, demonstrating an adequate impregnation of the wax through the substrate to the opposite surface, in relation with the contact angle results (Figures 3c and 3d). The addition of fillers to the wax has a larger morphological influence on the cross-section. In fact, while the surface remains rough and hydrophobic with the addition of fillers to the wax (Figures 4c and 4d), the larger the concentration of fillers, the larger the thickness presented by the samples (Figures 4g and 4h). This result demonstrates that GNP present difficulty to cross the substrate and remains mostly on the substrate surface, which may be due to the combined effect of the GNP dimensions and the fibrillar paper substrate with reduced pore size, resulting on a very compact layer of composite wax at the surface of the substrate. Nonetheless, as demonstrated in the contact angle results (Figures 3c and 3d) and in the proofs of concept discussed later (Section 3.2), the hydrophobic barriers needed to contain fluids are guaranteed.

To evaluate how the printing process and the corresponding thermal treatment (curing process) affects the mechanical properties of the printed substrates, peeling assays on 10×10 mm samples (Figures 5a and 5b) and stress-strain measurements on 10×30 mm samples (Figures 5c and 5d) in tensile mode were carried out[2]. Uncured prints can find application when the conductive waxes, i.e. heater, do not need to cross the entire substrate and work as fluid barriers, as occurred in the second proof of concept. However, it can negatively affect the mechanical properties, as it will be shown in the following, so that the need for curing must be properly evaluated according to the application.

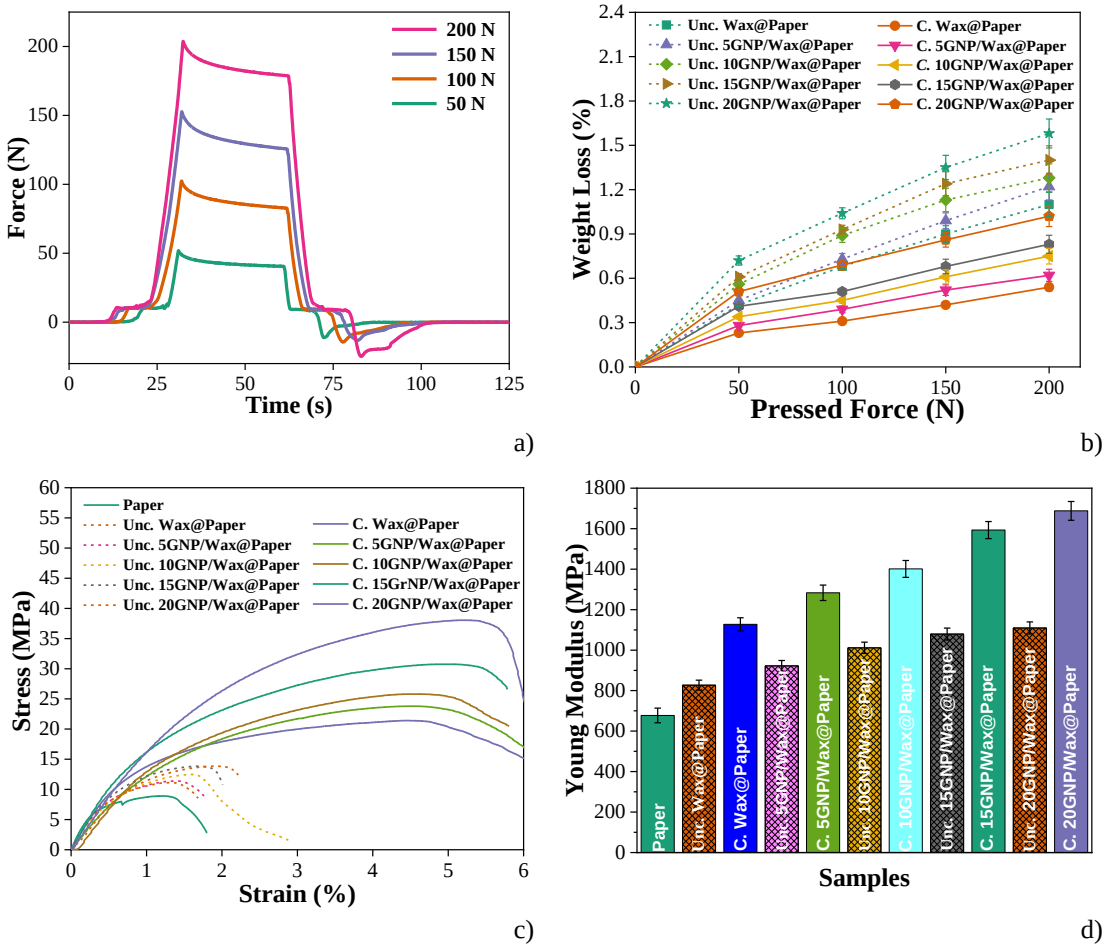

Figure 5: a) Force profile of the peeling assays for the various wax printed samples as a function of time and compression force; b) respective weight loss after the peeling assays as function of the compression force. c) Stress-strain curves for the various wax printed samples obtained at room temperature; d) respective Young's modulus values obtained from c).

The force profile during the peeling assays for the printed layers (Figure 5a) shows that the lowest compression force of 50 N leads to the lowest peeling force of ~11 N, while the highest compression force of 200 N leads to the highest peeling force of ~25 N. Regarding Figure 5b, it is shown that increased compression forces lead to increased

weight loss, regardless the sample. Moreover, the benefits of thermal treatment on the stability of the wax print are demonstrated, with less weight loss in the cured samples. A maximum of ~1 % is loss for the cured 20 wt.% GNP/Wax at a compression force of 200 N (~1.6 % for the respective uncured sample) whereas a maximum of ~0.3 % is loss in the case of cured 5 wt.% GNP/Wax (~0.5 % for the respective uncured), very close to the value of ~0.2 % for the cured neat wax (~0.4 % for the respective uncured). Although some weight loss is evidenced, which is more pronounced for high compression forces and uncured waxes, the results confirm the mechanical stability of the printed waxes, as the observed weight loss does not compromises the mechanical and functional characteristics of the samples. Further, none of the samples experienced weight loss in a second round of assays. Accordingly, the proofs of concept will be performed using cured waxes.

The characteristic stress-strain curves of the processed samples (30 mm long and 10 mm wide) are presented in Figure 5c. From the liner regimes of the curves (until 0.5%), the Young's modules were obtained for each samples applying Hooke's law and the values are presented in Figure 5d. Commercial *Whatman nº1* paper features almost no plastic regime, with a fracture near the end of the linear elastic region of the curve. On the other hand, all printed paper samples present both higher stress and strain at the breaking point, demonstrating the mechanical reinforcement of the wax. This increase proves to be significantly higher when the wax is thermally cured, indicating a strong improvement of the mechanical properties. In fact, printed papers present maximum strain of 1.5 to 2 % of strain and 10 to 15 MPA of stress for uncured samples and between 5 to 5.5 % of strain and 20 to 40 MPa of stress at breaking point for cured samples. Moreover, comparable improvements are detected with the increase of the GNP concentration in the wax. The analysis of the Young modules obtained in the linear mechanical regime, where the materials are generally used, allow to reinforce the previously mentioned conclusions. In fact, increasing GNP concentration in the wax leads to higher Young's modules, the increase being much more significant when the wax is cured. An increase of ~67 % is obtained in the cured wax compared to the neat paper. Moreover, the addition of 20 wt.% GNP to the wax and the curing process allows an increase of ~49% compared the cured neat wax and ~148 % compared to the neat paper. Regarding the relevance of thermal curing in the mechanical properties and analysing the samples composed by 20 wt.% GNP/Wax, an increase of ~53 % is obtained after curing. The increase of the Young's

modulus can thus be explained by the impregnation of wax in the fibrillary structure of the *Whatman nº1* paper in combination with the addition of GNP fillers (with a large Young's modulus of 20-60 GPa[59]) and the corresponding filler-matrix interaction.

The electrical and thermal performance of wax and the corresponding composites up to 20 wt.% are presented in Figure 6. The sheet electrical resistance is presented in Figure 6a.

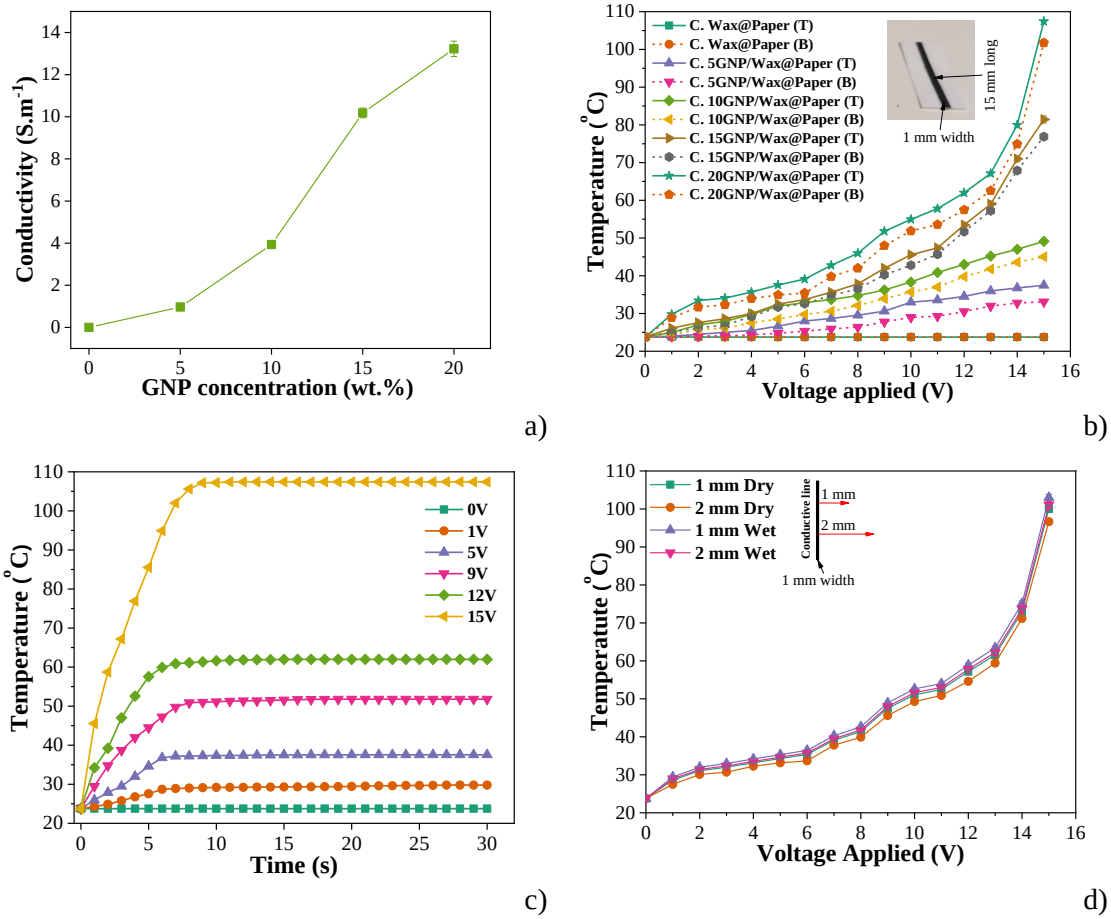

Figure 6: a) Electrical conductivity values of the various wax based printed samples as a function of GNP concentration. b) Temperature at the top (T) and bottom (B) of the different GNP/Wax lines (15 mm long and 1 mm width) printed and cured on *Whatman nº1* paper as function of the applied voltage. c) Temperature variation as a function of time for various applied voltages measured at the top of the printed and cured 20 wt.% GNP/Wax lines. d) Temperature measured at the top of the substrate in the dry and wet state as function of the applied voltage, 1 and 2 mm away from the printed and cured 20 wt.% GNP/Wax lines.

The electrical conductivity of the neat wax is near 2.1×10^{-12} S.m^{-1} increasing about 12 orders of magnitude with increasing filler content up to a value of ~13.2 S.m^{-1} for the sample with a filler content of 20 wt.%. This increase in the electrical conductivity will

have a direct effect on the generated heat capacity, as described in the following. Thus, the focus rely on high-filled composites, leading to larger graphene content and lower electrical resistance, leading also to properly tune the thermal heating of the composites[60]. The obtained percolations threshold, on the other hand, is in line with the literature with related composites[61]. Moreover, it should be also highlighted that no significant variation in the electrical conductivity is verified after peeling tests.

By means of a temperature probe, thermal measurements at the top and bottom of the different GNP/Wax lines (15 mm long and 1 mm width) printed and cured on *Whatman nº1* paper were measured as function of the electrical voltage, after 30 s (Figure 6b). No heating is generated by neat wax, regardless the measuring surface. On the other hand, in all wax composites, the higher the applied voltage, the higher the heating generated by the conductive lines. The temperature increase shows to be higher on the upper surface of the printed line (T), i.e. top surface of the substrate, compared to the inner surface of the line (B), i.e. bottom surface of the substrate, which confirms that there is a higher accumulation of GNP fillers on the surface of the print, as previously demonstrated in the contact angle measurements (Figure 3d) and SEM images (Figures 4g and 4h). A maximum temperature of ~107 ºC was measured at the top of the cured 20 wt.% GNP/Wax line (~102 ºC below) for an applied voltage of 15 V, while a value of ~37 ºC was obtained at the top of the cured 5 wt.% GNP/Wax line (~32 ºC below) for the same applied voltage. Higher voltages were not evaluated due to the thermal sensitivity of the *Whatman Nº1* substrate, which is based on cellulose. However, more thermally resistant membranes, such as PVDF and their copolymers [8,62], can be an option if higher heating is required. Applying the voltage with alkaline batteries of 1.5, 9 and 12 V, temperatures of ~31.5, 51.6 and 62.1 ºC were obtained at the top of the cured 20 wt.% GNP/Wax lines, respectively. These results are interesting for applications in several fields, previously evidenced, since it is demonstrated that it is possible to adjust and control the heating generated through the proper selection of the applied electrical signal and/or the concentration of GNP fillers in the wax.

Another interesting conclusion illustrated in Figure 6c is that the maximum temperature is achieved in a few seconds (~9 s), remaining stable over time. Figure 6c reports on 20 wt.% GNP printed lines (1 mm width) after curing.

Finally, temperature was measured after 10 s at a fixed distance from the conducting lines, namely at 1 and 2 mm to evaluate the heat loss through the paper. The results are shown

in Figure 6d for a conducting line of cured 20 wt.% GNP/Wax (1 mm width). These dimensions were chosen considering that in µPADs, the channels have a very small width (mm or below) in order to allow adequate passive flows without the need for external pumps or pressure. Comparing with the results presented in Figure 6b, it is concluded that there is a small heat transfer, which is more accentuated when the paper is dry when compared to the wet state. This is explained by the fact that wet paper feature a higher thermal conductivity than dry paper, respectively [63,64]. For the maximum applied voltage of 15 V, a temperature variation of ~4 and ~7ºC (from the initial ~107 ºC at the top of the line) occurs at a distance of 1 mm from the line in the wet and dry states, respectively. At a distance of 2 mm, the temperature variation presents values of ~6 and ~10 ºC in the wet and dry state, respectively. Those variations have to be taken into consideration when precise temperature control is required and µPADs design and dimensions have to be optimized to account for those temperature gradients.

3.2. Functional proofs of concept validation

Thermochromic inks have the ability to change colour when heated above a certain temperature. This concept was employed in µPADs devices made of *Whatman nº1* paper substrates and patterned using printed and cured neat wax and 20 wt.% GNP/Wax lines (Figure 7a). In this system, red and green thermochromic inks were used, changing to more translucent (light rose) and yellow at temperatures higher than 47 and 28 ºC, respectively (Figure 7b). Different conductive lines were activated by means of a DC power supply at 12 V (Figure 7c) and 14 V (Figure 7d).

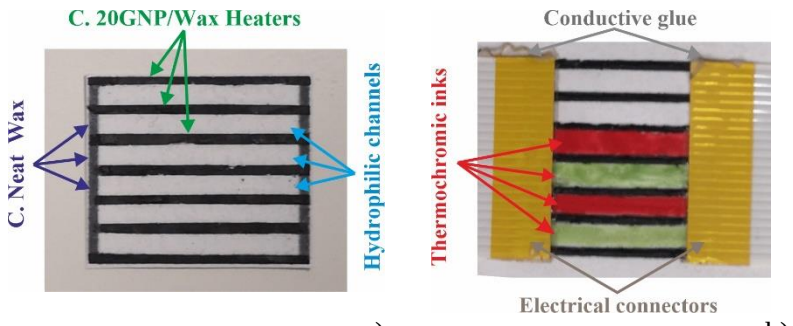

a) b)

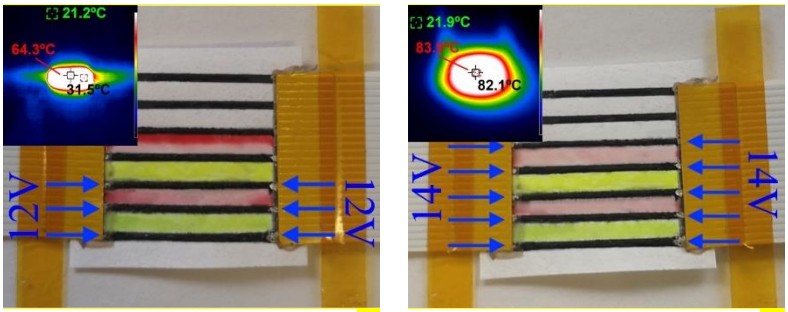

Figure 7: Photographs of a) µPADs system with individual hydrophilic channels delineated by printed and cured hydrophobic neat wax and hydrophobic conductive 20 wt.% GNP/Wax lines; b) Two thermochromic inks at room temperature (red activated at 47 ºC and green activated at 28 ºC); Resulting colour changes when specific conductive lines are subject to an electrical voltage of c) 12 V and d) 14V indicated by the blue arrows. Corresponding thermal images in inset.

At room temperature (~25 ºC), the thermochromic inks feature a clear green and red colour (Figure 7b). When a voltage of 12 V is applied to the three lower conductive lines, a maximum temperature of ~64.3 ºC was measured using the thermal imaging camera, near the ~61.9 ºC obtained by means of the temperature probe (Figure 7c). This result in a colour change of the inks presented in the three lower channels, meaning that the thermochromic activation temperatures are reached. On the other hand, the upper channel features a clear colour gradient from translucent red to bright red (light rose) also indicating a temperature gradient between values above and below the activation temperature. Thus, it becomes evident that there is a reduction in temperature with increasing distance between the reaction channel and the superior conductive line, as expected and previously concluded in Figure 6d. When the voltage is increased to 14 V and applied to the four lower conductive lines (Figure 7d), all inks undergo colour changes, with a maximum temperature of ~83.9 ºC measured with the thermal imaging camera, near the ~80.1 ºC obtained using the temperature probe, much higher than the activation temperature of both thermochromic inks.

To further strengthen the capabilities of the manufactured materials as well as their suitability for µPADs applications, a second proof of concept was carried out using alkaline batteries of 1.5, 9 and 12 V instead of a DC power supply. For that, a 3D printed support was manufactured to include the battery inside and protect it from possible moisture and short circuit. The disposable µPADs consist on a folded *Whatman nº1* paper with a rectangular heater made of 20 wt.% GNP/Wax underneath a circular testing area delimitated by neat wax, where the thermochromic ink is placed (Figure 8a). Although

there was no need for post-thermal cure of the conductive wax since in this case it works only as heater, the entire system was cured to increase the mechanical stability of the printed waxes and thus of the µPADs, as concluded in Figures 5a and b. In this case, two red thermochromic inks were used with activation temperatures at 28 ºC (Figure 8b) and 47 ºC (Figure 8c), respectively.

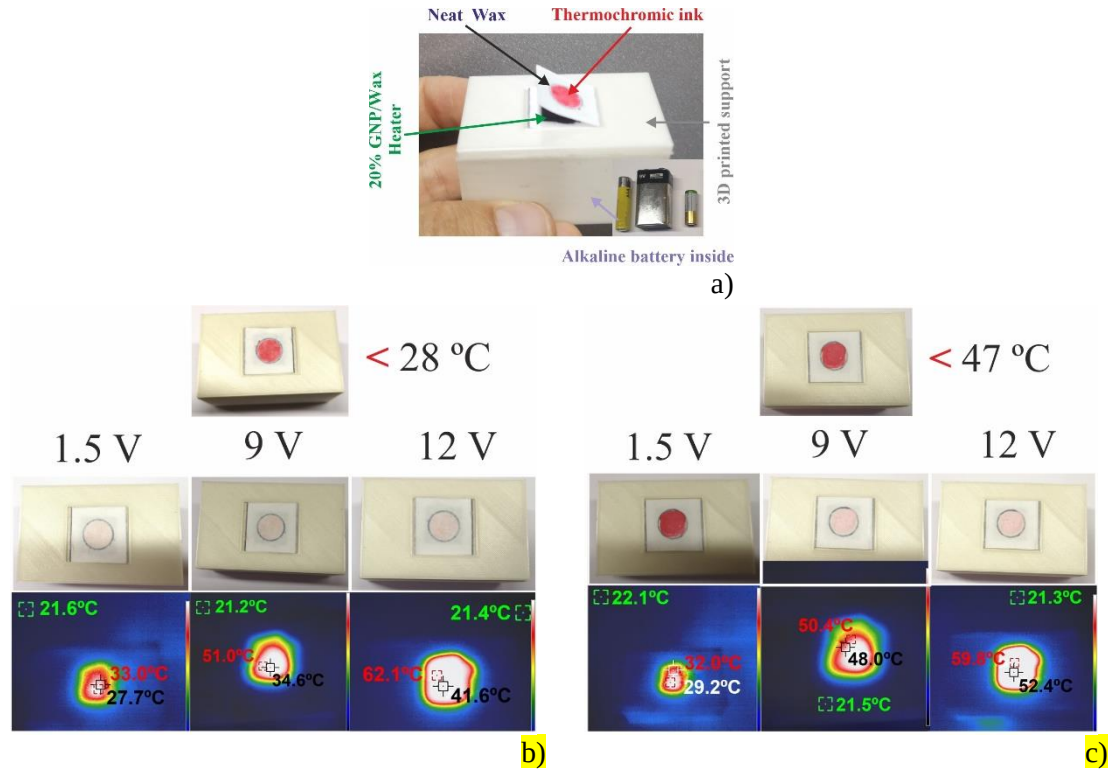

Figure 8: Photographs of a) portable printed folded *Whatman nº1* paper devices, in which a battery (1.5, 9 or 12 V) placed inside the 3D printed support is connected to a 20 wt.% GNP/Wax square, in order to provide heat to the thermochromic ink contained in the circular testing area delimited by neat wax; b) thermochromic ink (activated at 28 ºC) with conductive square subjected to a voltage of 1.5, 9 and 12 V and corresponding thermal images; c) thermochromic ink (activated at 47 ºC) with conductive square subjected to a voltage of 1.5, 9 and 12 V and corresponding thermal images.

Regarding the results presented in Figure 8b, the ink with an activation temperature of 28 ºC changes colour regardless the battery used from a bright red to a more translucent red (light rose.) At 1.5 V, 9 and 12 V applied voltages, maximum temperatures of ~32.0, 50.5 and ~59.8 ºC are measured using the thermal imaging camera, close to the values of ~31.5, 51.6 and 62.1 ºC obtained by means of the temperature probe (Figure 6b), respectively, which are higher than the activation temperature of the ink, which is in line with the obtained results. On the other hand, the heating generated by the 1.5 V battery is not enough to change the colour of the ink with an activation temperature of 47 ºC, as shown in Figure 8c. The two batteries with higher potential allow to generate enough temperature variation for a colour transition, with the values previously described.

These aforementioned proofs of concept can be further tailored according to the application, e.g. by varying µPADs design, GNP/Wax concentration, or applied voltage, but nevertheless convincingly validate the concept of multifunctional conductive waxes development for portable µPAD systems, allowing to work simultaneously as hydrophobic barriers and heaters, using a simple, rapid and low cost fabrication method with reproducible response.

4. Conclusions

This work reports on the development of multifunctional waxes based on the integration of conductive graphene nanoplatelets (GNP) into the wax matrix for microfluidic paper-based analytical device (µPAD) applications. This approach allows the wax to work simultaneously as hydrophobic barriers, its commonly used property to delimit boundaries into hydrophilic paper substrates, and also as heater for temperature-sensitive applications. The process of wax patterning in paper involves a single, simple and fast printing method allowing cost-effective tailorable production. Moreover, portability is assured by the possibility of using lightweight and low-power actuation systems such as alkaline batteries. Wax prints with mechanical stability and adequate impregnation through the paper were obtained after proper post-thermal curing. Tailorable temperatures ranging from room temperature to ~107 ºC were achieved by varying GNP weight content up to 20 wt.% and applied electric potential up to 15 V. Moreover, thermochromic inks with the ability to change colour above a certain activation temperature were used in pre-designed and printed wax-based µPADs to validate heating reproducibility and low-power thermal actuation.

The proposed printable wax composites with improved functionality and performance, allied to the benefits of µPADs, provide a novel and simple solution to meet the increased requirements of complex multi-step analysis, with the ultimate goal of promoting their standardization and further commercialization.

Acknowledgments

The authors thank the FCT- Fundação para a Ciência e Tecnologia- for financial support in the framework of the Strategic Funding UID/FIS/04650/2020, UIDB/04436/2020,

UIDP/04436/2020. RBP and PC thank support from FCT under SFRH/BD/140698/2018 and SFRH/BPD/110914/2015 grants, respectively. CR and VFC thank the FCT for the contracts under the Stimulus of Scientific Employment 2020.04163.CEECIND, 2020.02304.CEECIND, respectively, and VC for the junior researcher contract DL57/2016. Finally, the authors acknowledge funding from the Basque Government Industry Department under the ELKARTEK programs.

References

[1] K. Ratajczak, M. Stobiecka, *Carbohydr. Polym.* **2020**, *229*.

[2] Y. Xia, J. Si, Z. Li, *Fabrication techniques for microfluidic paper-based analytical devices and their applications for biological testing: A review*, Vol. 77, Elsevier Ltd, **2016**, pp. 774–789.

[3] M. Sher, R. Zhuang, U. Demirci, W. Asghar, *Expert Rev. Mol. Diagn.* **2017**, *17*, 351.

[4] E. Noviana, C. P. McCord, K. M. Clark, I. Jang, C. S. Henry, *Lab Chip* **2020**, *20*.

[5] A. W. Martinez, S. T. Phillips, M. J. Butte, G. M. Whitesides, *Angew. Chemie* **2007**, *119*, 1340.

[6] M. C. C. G. Carneiro, L. R. Rodrigues, F. T. C. Moreira, M. G. F. Sales, *Sensors* **2022**, *22*.

[7] E. S. Pimentel, R. Brito-Pereira, T. Marques-Almeida, C. Ribeiro, F. Vaz, S. Lanceros-Mendez, V. F. Cardoso, *ACS Appl. Mater. Interfaces* **2020**, *12*, 60.

[8] R. Brito-Pereira, A. S. Macedo, C. R. Tubio, S. Lanceros-Méndez, V. F. Cardoso, *ACS Appl. Mater. Interfaces* **2021**, *13*, 18065.

[9] R. Brito-Pereira, A. S. Macedo, C. Ribeiro, V. F. Cardoso, S. Lanceros-Méndez, *Appl. Mater. Today* **2022**, *28*.

[10] R. Brito-Pereira, C. Ribeiro, S. Lanceros-Méndez, V. Fernandes Cardoso, *Chem. Eng. J.* **2022**, *448*.

[11] V. Busin, B. Wells, M. Kersaudy-Kerhoas, W. Shu, S. T. G. Burgess, *Opportunities and challenges for the application of microfluidic technologies in point-of-care veterinary diagnostics*, Vol. 30, Academic Press, **2016**, pp. 331–341.

[12] S. A. Papatheodorou, T. Tsironi, M. Giannakourou, P. Halvatsiotis, D. Houhoula, *J. Sci. Food Agric.* **2022**.

[13] N. Yang, K. Shen, J. Guo, X. Tao, P. Xu, H. Mao, In *Modern Physics Letters B*, **2017**.

[14] G. Musile, Y. Agard, L. Wang, E. F. De Palo, B. McCord, F. Tagliaro, *Paper-based microfluidic devices: On-site tools for crime scene investigation*, Vol. 143, **2021**.

[15] F. Sharifi, S. Ghobadian, F. R. Cavalcanti, N. Hashemi, *Paper-based devices for energy applications*, Vol. 52, **2015**.

[16] N. A. Meredith, C. Quinn, D. M. Cate, T. H. Reilly, J. Volckens, C. S. Henry, *Analyst* **2016**, *141*, 1874.

[17] J. Adkins, K. Boehle, C. Henry, *Electrophoresis* **2015**, *36*, 1811.

[18] L. M. Fu, Y. N. Wang, *Detection methods and applications of microfluidic paper-based analytical devices*, Vol. 107, **2018**.

[19] S. Smith, J. G. Korvink, D. Mager, K. Land, *RSC Adv.* **2018**, *8*, 34012.

[20] W. Y. Lim, B. T. Goh, S. M. Khor, *Microfluidic paper-based analytical devices for potential use in quantitative and direct detection of disease biomarkers in clinical analysis*, Vol. 1060, **2017**.

[21] B. Selvakumar, A. Kathiravan, *Talanta* **2021**, *235*.

[22] H. Lim, A. T. Jafry, J. Lee, *Molecules* **2019**, *24*.

[23] W. Mazurkiewicz, M. Podrażka, E. Jarosińska, K. Kappalakandy Valapil, M. Wiloch, M. Jönsson-Niedziółka, E. Witkowska Nery, *Paper-Based Electrochemical Sensors and How to Make Them (Work)*, Vol. 7, **2020**.

[24] S. Atabakhsh, Z. Latifi Namin, S. Jafarabadi Ashtiani, *Microsyst. Technol.* **2018**, *24*.

[25] M. Franco, R. Alves, N. Perinka, C. Tubio, P. Costa, S. Lanceros-Mendéz, *ACS Appl. Electron. Mater.* **2020**, *2*, 2857.

[26] N. Karim, M. Zhang, S. Afroj, V. Koncherry, P. Potluri, K. S. Novoselov, *RSC Adv.* **2018**, *8*, 16815.

[27] D. Zhang, C. Li, D. Ji, Y. Wang, *Paper-Based Microfluidic Sensors for Onsite Environmental Detection: A Critical Review*, Vol. 52, **2022**.

[28] T. Akyazi, L. Basabe-Desmonts, F. Benito-Lopez, *Anal. Chim. Acta* **2018**, *1001*, 1.

[29] S. Sachdeva, R. W. Davis, A. K. Saha, *Microfluidic Point-of-Care Testing: Commercial Landscape and Future Directions*, Vol. 8, **2021**.

[30] J. C. Brooks, C. R. Mace, *Scalable Methods for Device Patterning as an Outstanding*

Challenge in Translating Paper-Based Microfluidics from the Academic Benchtop to the Point-of-Care, Vol. 3, **2019**.

[31] X. Jiang, Z. H. Fan, *Fabrication and Operation of Paper-Based Analytical Devices*, Vol. 9, **2016**.

[32] G. Sriram, M. P. Bhat, P. Patil, U. T. Uthappa, H. Y. Jung, T. Altalhi, T. Kumeria, T. M. Aminabhavi, R. K. Pai, Madhuprasad, M. D. Kurkuri, *Paper-based microfluidic analytical devices for colorimetric detection of toxic ions: A review*, Vol. 93, **2017**.

[33] H. R. Singhal, A. Prabhu, M. S. Giri Nandagopal, T. Dheivasigamani, N. K. Mani, *One-dollar microfluidic paper-based analytical devices: Do-It-Yourself approaches*, Vol. 165, **2021**.

[34] T. Han, Y. Jin, C. Geng, A. ur R. Aziz, Y. Zhang, S. Deng, H. Ren, B. Liu, *Microfluidic Paper-based Analytical Devices in Clinical Applications*, Vol. 83, **2020**.

[35] S. Altundemir, A. K. Uguz, K. Ulgen, *Biomicrofluidics* **2017**, *11*.

[36] V. F. Cardoso, T. Knoll, T. Velten, L. Rebouta, P. M. Mendes, S. Lanceros-Méndez, G. Minas, *RSC Adv.* **2014**, *4*.

[37] H. F. Chang, S. E. Chou, J. Y. Cheng, *J. Vis. Exp.* **2021**, *2021*.

[38] M. Kojima, M. Horade, S. Takata, S. Nakadai, Y. Mae, T. Arai, In *2017 IEEE International Conference on Cyborg and Bionic Systems, CBS 2017*, **2017**.

[39] S. H. Hong, J. Il Shu, Y. Wang, O. Baysal, *Biomed. Microdevices* **2021**, *23*.

[40] D. S. Lee, O. R. Choi, Y. Seo, *Micro Nano Syst. Lett.* **2019**, *7*.

[41] N. Privorotskaya, Y. S. Liu, J. Lee, H. Zeng, J. A. Carlisle, A. Radadia, L. Millet, R. Bashir, W. P. King, *Lab Chip* **2010**, *10*.

[42] A. V. Govindarajan, S. Ramachandran, G. D. Vigil, P. Yager, K. F. Böhringer, *Lab Chip* **2012**, *12*.

[43] S. Mondal, V. Venkataraman, *J. Biochem. Biophys. Methods* **2007**, *70*.

[44] J. Chen, Y. Wang, F. Liu, S. Luo, *ACS Appl. Mater. Interfaces* **2020**, *12*.

[45] G. Wang, L. Q. Tao, T. Li, Z. Peng, C. Zhu, S. Zou, H. Sun, X. Chen, *IEEE Electron Device Lett.* **2022**, *43*.

[46] K. A. Hagan, C. R. Reedy, M. L. Uchimoto, D. Basu, D. A. Engel, J. P. Landers, *Lab Chip* **2011**, *11*.

[47] K. J. Shaw, P. T. Docker, J. V. Yelland, C. E. Dyer, J. Greenman, G. M. Greenway, S. J. Haswell, *Lab Chip* **2010**, *10*.

[48] Y. Ohtsu, R. Yamada, H. Urasaki, T. Misawa, S. Popescu, H. Fujita, *J. Mater. Cycles Waste Manag.* **2010**, *12*.

[49] N. S. Jang, K. H. Kim, S. H. Ha, S. H. Jung, H. M. Lee, J. M. Kim, *ACS Appl. Mater. Interfaces* **2017**, *9*.

[50] S. Atabakhsh, S. Jafarabadi Ashtiani, *Microfluid. Nanofluidics* **2018**, *22*.

[51] H. Fang, S.-L. Bai, C. P. Wong, *Compos. Part A Appl. Sci. Manuf.* **2018**, *112*, 216.

[52] A. Li, C. Zhang, Y.-F. Zhang, *Polymers (Basel).* **2017**, *9*.

[53] W. H. Danial, Z. Abdul Majid, *Carbon Lett.* **2022**, *32*, 1411.

[54] M. Silva, S. G. Caridade, A. C. Vale, E. Cunha, M. P. Sousa, J. F. Mano, M. C. Paiva, N. M. Alves, *RSC Adv.* **2017**, *7*.

[55] H. S. Kim, H. S. Bae, J. Yu, S. Y. Kim, *Sci. Rep.* **2016**, *6*.

[56] R. Brito-Pereira, C. R. Tubio, P. Costa, S. Lanceros-Mendez, *Compos. Sci. Technol.* **2021**, *213*.

[57] R. Brito-Pereira, C. R. Tubio, S. Lanceros-Mendez, P. Martins, *Adv. Mater. Technol.* **2021**, *6*.

[58] R. Brito-Pereira, C. Ribeiro, N. Pereira, S. Lanceros-Mendez, P. Martins, *Nano Energy* **2022**, *94*.

[59] C. Feng, Y. Wang, J. Yang, *Nanomaterials* **2018**, *8*.

[60] V. Orts Mercadillo, K. C. Chan, M. Caironi, A. Athanassiou, I. A. Kinloch, M. Bissett, P. Cataldi, *Adv. Funct. Mater.* **2022**, *32*.

[61] X. Wu, P. Steiner, T. Raine, G. Pinter, A. Kretinin, C. Kocabas, M. Bissett, P. Cataldi, *Adv. Electron. Mater.* **2020**, *6*.

[62] C. Ribeiro, C. M. Costa, D. M. Correia, J. Nunes-Pereira, J. Oliveira, P. Martins, R. Gonçalves, V. F. Cardoso, S. Lanceros-Méndez, *Nat. Protoc.* **2018**, *13*, 681.

[63] S. A. Lavrykov, B. V. Ramarao, *Dry. Technol.* **2012**, *30*.

[64] F. Szodrai, Á. Lakatos, *Build. Serv. Eng. Res. Technol.* **2017**, *38*.

Conductive graphene nanoplatelets (GNP) integrated into wax matrix are developed to work as printable multifunctional materials, i.e. hydrophobic barrier and heater simultaneously, for microfluidic paper-based analytical device (µPAD) applications. Wax prints with mechanical stability, adequate impregnation and tailorable temperatures ranging from room temperature to ~107 ºC are achieved, providing a novel and simple solution to meet complex multi-step analysis requirements.

R. Brito-Pereira, C. Ribeiro, P. Costa, V. Correia, V. F. Cardoso* and S. Lanceros-Mendez*

Graphene based printable conductive wax for low-power thermal actuation in microfluidic paper-based analytical devices